13. GROUP OF GAS DISCHARGES AND GASEOUS ELECTRONICS

C. M. Ferreira (Head), L. Alves, F.M. Dias, V. Guerra, J. Henriques, S. Letout, J. Loureiro, L. Marques, L. Novo, M. Pinheiro, E. Tatarova.

13.1. INTRODUCTION

This Group carried out activities in 2004 mainly related with two research areas:

- Environment plasma engineering;
- Modelling of plasma reactors.

13.2. ENVIRONMENT PLASMA ENGINEERING LABORATORY

13.2.1. Introduction

Having in view environmental issues, the main activity of the "Gaseous Electronics" research group during 2004 was focused on detailed experimental and theoretical investigations of large-scale microwave molecular plasmas. Plasma sources operating in N_2, O_2, H_2 and their mixtures are presently the subject of many investigations due to their importance in plasma-based technologies and in atmospheric physics. For example, gas discharges operating in nitrogen-oxygen mixtures are used for cold sterilization of medical devices, removal of nitrogen oxides (NO_x) from flue and exhaust gases. Nitrogen-hydrogen mixtures are important as sources of ground state atoms. Large-scale plasma sources based on microwave propagation are of interest for new-generation technologies because of the high number densities of active species they yield. The effect of the plasma in the treatment process is strongly correlated with the spatial distribution of the species and the plasma parameters, as is well known.

13.2.2. Experiment

13.2.2.1. Experimental system development

An improvement in the operation of the large-scale plasma source has been done during 2004. A schematic diagram of the plasma source is shown in Figure 13.1. The discharge chamber is a stainless steel tube (d = 30 cm) headed by a water-cooled aluminium block and closed at the top by a 10 mm-thick quartz window. A 2.45 GHz microwave power supply is coupled to the plasma using a pair of slot antennas formed on a waveguide base plane. The generator is isolated from the discharge chamber by a high power circulator with high power matched load used for matching the impedance of the discharge chamber to the waveguide.

The plasma is created by the energy carried by surface waves propagating radially (r) and azimuthally (φ) along the interface between the plasma and a quartz dielectric plate located at the top wall. In the discharge, two different zones are formed due to the exponential decrease of the electric field. The first one is the active discharge zone close to the interface, where the surface waves propagate and sustain the discharge, and the second one is the remote, "electric field-free" plasma zone (Figure 13.1).

In order to get spatial resolution of the emission spectroscopy measurements, an "optical periscope" system has been designed and constructed. The "optical periscope" is placed inside the plasma (Figure 13. 2).

Figure 13.1 – Large-scale source: experimental set-up.

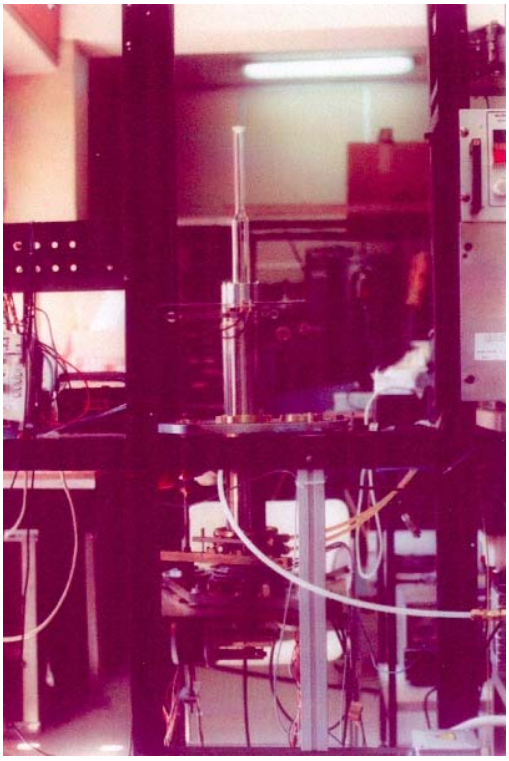

Figure 13.2 - "Optical periscope"

It consists of a hollow stainless steel piston with an optical fibre located inside. The piston is terminated at the top by an optical quality window and a right-angle prism. The "periscope" can be moved in the axial and azimuthal directions. The plasma radiation impinging radially on the prism is deflected towards the axis, collimated by a lens and then collected by the optical fibre, which guides it into the input slit of a spectrometer. The volume of plasma under investigation is determined by the apparatus function. Photons emitted by the plasma are transferred by the optical system into the entrance slit of a SPEX 1250M spectrometer (2400 g/mm grating) with a Hamamatsu R928 photomultiplier. The current generated by the photomultiplier is sent to data acquisition electronics DataScan2, and processed by Spectramax software.

13.2.2.2. Surface mode identification

An electrodynamical analysis of the plasma source has been performed. The waves form a resonant eigenmode satisfying the pertinent boundary conditions and the plasma takes discrete density values, which ensure that the resonant eigenmodes exactly appear at the excitation frequency (2.45 GHz). Selective excitation of a proper mode is necessary for stable operation of the system. For this reason, spatially resolved 3D measurements of the electric field components are performed and compared with the theoretical results to identify the mode sustaining the discharge. Electric field measurements have been performed by using a 0.5 mm tungsten wire probe (of length l = 5 mm), which is movable in the azimuthal (φ), radial (r), and axial (z) directions.

The 2D (azimuthal and radial) total electric field intensity pattern at a constant axial distance z=0.3 cm is depicted in Figure 13.3. The experimentally obtained azimuthal distribution of the radial electric field component, measured at fixed axial z and radial r positions, is shown in Figure 13.4. As seen, the measured distributions of the field components clearly correspond to the transverse magnetic TM_{330} mode, as considered theoretically.

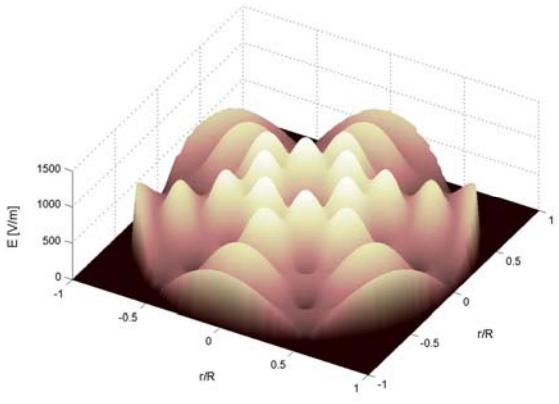

Figure 13.3 - 2D (r-φ) distribution of the total electric field.

13.2.2.3. Emission spectroscopy measurements

13.2.2.3.1. Emission from radiative states

Emission spectroscopy was used to measure the $N_2(C^3\Pi_u)$, $N_2^+(B^2\Sigma_u)$ and NO(γ) band intensities and the emission of excited hydrogen atoms [H_δ, H_γ], as a function of the spatial position in N_2–xO_2 and N_2–xH_2 , He–xH_2 mixtures[1].

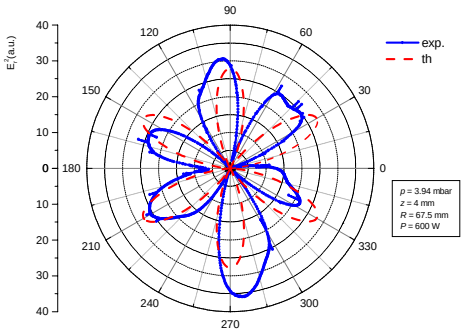

Figure 13.4 - Azimuthal variation of the square of the measured radial component of the electric field (z = 4 mm, r = 67.5 mm, p = 3 Torr).

The experimental data are discussed in the framework of kinetic considerations. The investigated intensity of the emission lines of the 2nd positive and 1st negative systems of N_2, and of NO(γ) and hydrogen atoms in the discharge zone of a large-scale N_2-O_2 and N_2-H_2 plasma source follows the spatial variation of the local electric field peculiar for the TM_{140} surface mode, as the obtained results demonstrate. On the contrary, the population in vibrational and rotational levels of the $N_2(C^3\Pi_u, v)$ state is spatially homogeneous. The vibrational spectrum of the NO(γ) band [$NO(A^2\Sigma^+, v' \rightarrow X^2\Pi, v'')$] has been detected in the UV range, between 230 and 290 nm. As seen from Figure 13.5 the azimuthal variations of the band head intensities of the lines corresponding to different vibrational transitions follow the variations in electric field intensity (TM_{140} mode) in the discharge zone.

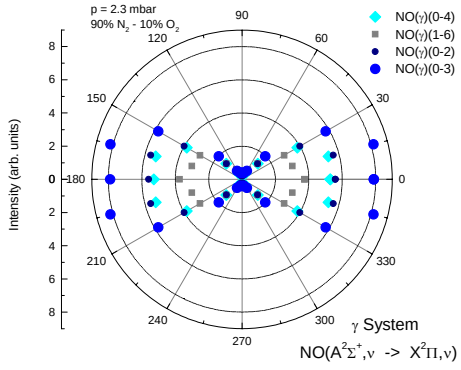

Figure 13.5 - Azimuthal variations of the band head intensities corresponding to different vibrational transitions of the NO(γ) system (Δz = 1 cm).

[1] Work carried out in collaboration with CPAT-URS (France), and the Lebedev Physical Institute of the Russian Academy of Sciences (Rússia).

13.2.2.3.2. Gas heating

The rotational distribution of the intensity of the R-branch in the $N_2(C^3\Pi_u, v'=0 \rightarrow B^3\Pi_g, v''=2)$ band of N_2 was used for temperature determination taking into account the Hönl-London factors. Because the measured distributions nearly follow Boltzmann´s law, the rotational temperature for the state can be introduced. The azimuthal distribution of T_r in the active plasma zone, i.e. close to the interface for two different N_2-O_2 mixture compositions is shown in Figure 6. As seen, the measured values are around 1000 K, independently of the azimuthal position. Thus, significant homogeneity of the rotational excitation of N_2 molecules is observed. Due to fast rotational–translational energy exchanges, these temperatures are also indicative of the gas temperature and of the spatial distribution of gas heating.

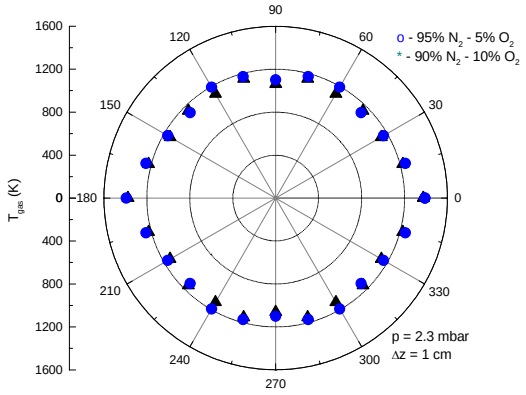

Figure 13.6 - Azimuthal distribution of T_r in a N_2-O_2 discharge.

13.2.2.3.3. Doppler broadening technique

The Doppler broadening technique has been applied to investigate a new effect associated with excessive broadening (and excess of energy generated) of the H_α atomic line in hydrogen containing mixtures, like Ar-H_2 and He-H_2. Recent spectroscopic diagnostics of He-xH_2 and H_2 plasmas generated by a slot antenna excited microwave plasma source, operating at $\omega/2\pi$=2.45 GHz, reveal that the emission profile of the Balmer-α line shows larger broadening than the Balmer-β and the helium line at 5875.7A [transition $3^3D \rightarrow 2^3P$] (Figure 13.7). The temperatures corresponding to the H_α and H_β lines profiles are 0.28 eV and 0.17 eV, respectively, much higher than the wall temperature and the rotational temperatures calculated from the Q-branch of the Fulcher-α band [$d^3\Pi_u$ (v=0) → $a^3\Sigma_g^+$ (v=0)] under the same conditions. The measured full width at half maximum (FWHM) of the H_α and H_β lines is nearly constant in the axial direction, i.e., does not change along the transition between the discharge and the remote plasma in He-H_2, (Figure 13.8).

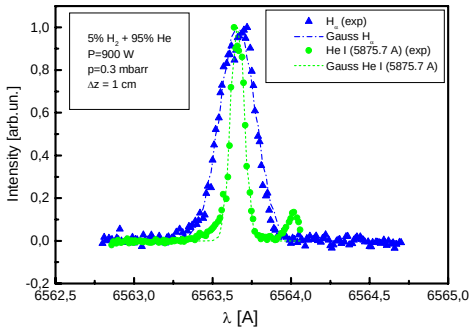

Figure 13.7 - Typical H_α, and helium 5875.7 A line profiles recorded in the discharge zone of a He-H_2 plasma.

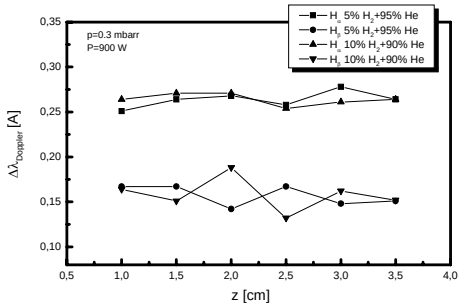

Figure 13.8 - Axial variation of FWHM of H_α and H_β lines in He-H_2 plasma.

13.2.3. Theoretical analysis

13.2.3.1. Large scale plasma source

A self-consistent numerical model for a large-scale Ar plasma source excited by a pure TM_{330} surface mode was developed and used to investigate the 3D spatial structure of the discharge during 2004[2]. The model is based on the solution of a coupled system of equations including the electron Boltzmann equation, the particle balance equations for all the relevant charged and neutral species, the gas thermal balance, and the equations describing the TM_{330} surface mode electrodynamics. Probe diagnostic techniques and radiophysics methods have been applied to validate the model predictions. The density distributions of plasma electrons, positive ions and electronically excited states of Ar atoms were shown to be strongly correlated with the electric field intensity distribution in the discharge zone, close to the plasma-dielectric interface (Figure 13.8). In fact, the spatial 3D distributions of these species in the discharge clearly follow the electric field pattern, demonstrating that electron collision processes play a dominant role in the active part of the plasma source. As observed, close to the interface the density distribution follows the field distribution; the maxima of the electron density coincide with those of the field. Azimuthal homogeneity at z = 25 mm, i.e. at the end of the discharge zone, is nearly achieved (Figure 13.9). It should be stressed that the experimental results confirm the main trends predicted by the model (Figure 13.10). To our knowledge these are the first experimental and theoretical results with 3D resolution concerning these plasma sources.

[2] Work carried out in collaboration with the Department of Electrical Engineering, Nagoya University (Japan).

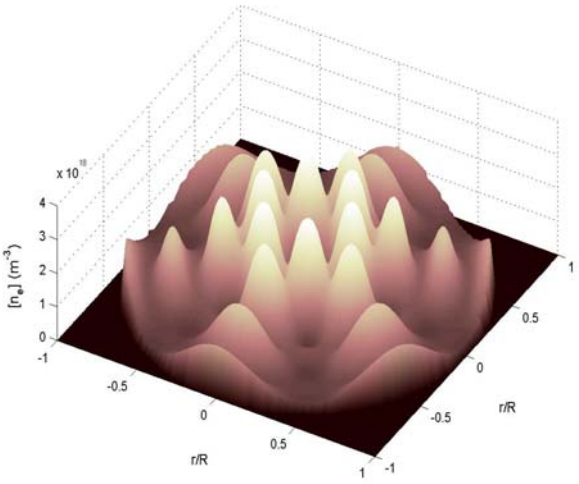

(z = 3 mm)

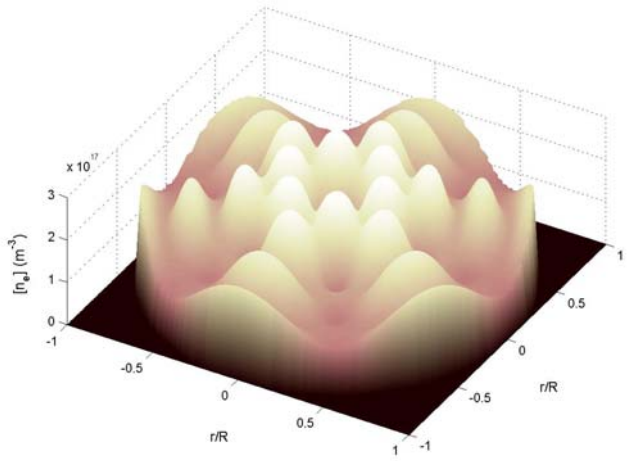

(z = 14 mm)

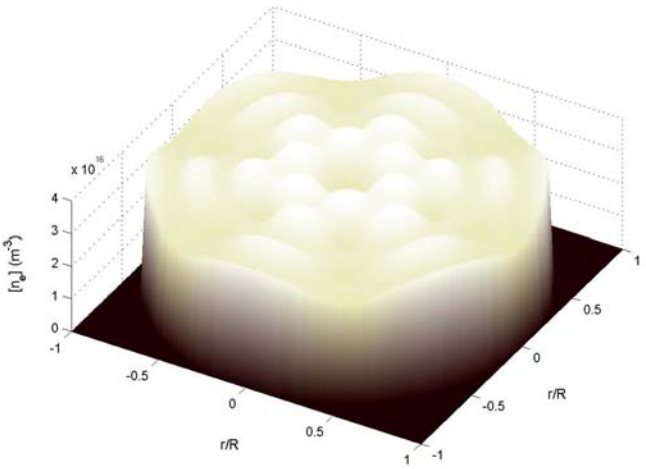

(z = 25 mm)

Figure 13.9 - 2D (r-φ) distribution of the electron density (a) z = 3 mm; (b) z = 14 mm; (c) z = 25 mm (p = 3 Torr, P = 600 W).

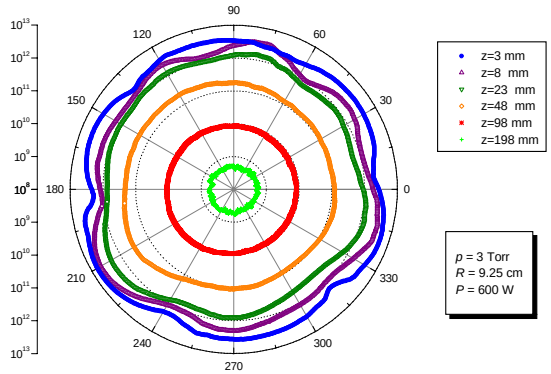

Figure 13.10 - Experimental axial dependence of the electron density azimuthal profile.

13.2.3.2. Afterglow studies

In recent years, there has been growing interest in the study of sterilization by afterglow plasmas due to the possibility of achieving such a process at relatively low temperatures. Plasma sterilization is an alternative to conventional sterilization systems in hospitals. Afterglows of flowing microwave discharges in N_2–O_2 to inactivate *Bacillus subtilis* spores have been the subject of preliminary studies by other groups[3]. It seems the spores are ultimately inactivated by UV photons, through destruction of their DNA strands. Simultaneously, the increased erosion of O_2 on the spores as time elapses reduces the number of photons required to reach the lethal dose. The action of O_2 probably results from the impinging of $O(^3P)$ atoms, while the action of UV radiation, as suggested by spectroscopic measurements, is due to the relatively strong intensity of the NOβ system bands (250–320 nm) emitted in the afterglow by NO(B) molecules. The major role attributed to UV photons in the sterilization process has also been confirmed.

In order to get physical insight into the processes occurring in these afterglow plasmas, we have developed detailed theoretical models first for pure nitrogen, which are currently being extended to N_2-O_2 . The kinetic model for the discharge starts with the determination of the electron energy distribution function (EEDF), the vibrational distribution functions (VDFs) of $N_2(X,v)$ and $O_2(X,v)$ molecules, the concentrations of N_2 and O_2 electronic states, N and O atoms, NO, NO_2 and O_3 species, and of the various positive and negative ions formed in the discharge. For atomic nitrogen, we consider both ground and excited states $N(^4S, ^2D, ^2P)$, whereas for oxygen we take into account atomic oxygen in the ground-state $O(^3P)$ only. Nitric oxides are also included with both ground and excited states, $NO(X, A, B)$ and $NO_2(X, A)$.

Figure 13.11 shows the calculated and measured concentrations of the first electronically excited metastable state $N_2(A)$ of nitrogen in the afterglow of a pure nitrogen microwave discharge operating at $(\omega/2\pi)$=433 MHz, in a Pyrex tube with inner radius R=1.9 cm, at a pressure p=440 Pa and flow rate Q=1.5 slpm. The data points were obtained by a French laboratory in Grenoble. This

[3] Work carried out in collaboration with the University of Montreal (Canada).

metastable state is an important energy carrier in the afterglow, and plays a crucial role in the post-discharge. It is very striking that an increase is observed in the population of $N_2(A)$ metastables in the field-free post-discharge. There must exist a local production of $N_2(A)$ molecules, which has been shown to be due to near resonant vibration-vibration (V-V) energy exchanges, followed by electronic-vibration (V-E) exchanges. The latter can be induced by collisions of highly vibrationally excited $N_2(X,v)$ molecules with both N atoms and electrons.

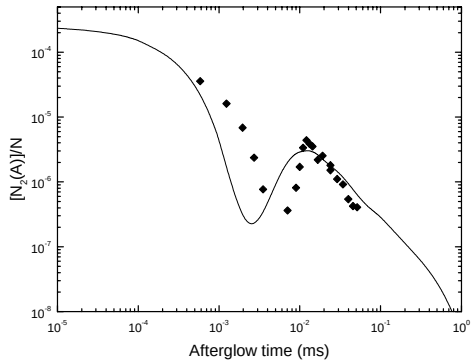

Figure 13.11 – Calculated and measured temporal evolution of the fractional concentration of $N_2(A)$ metastables in the afterglow of a microwave nitrogen discharge.

Once $N_2(A)$ states are created, they transfer energy to other states and to ionization. Therefore, many other excited states, as well as electrons and positive ions, have a similar profile during the afterglow. Figures 13.12 and 13.13 exhibit a comparison of calculations and measurements[4] for metastable $N(^2P)$ atoms and the radiative $N_2(B)$ state, respectively.

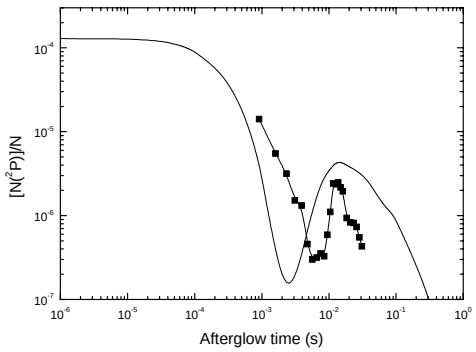

Figure 13.12 – Calculated and measured temporal evolution of the fractional concentration of $N(^2P)$ metastable in the afterglow of a microwave nitrogen discharge.

The detailed explanation of the energy transfers that take place in a nitrogen afterglow was a major achievement of our group. The knowledge obtained in the investigation of pure nitrogen plasmas is now being transferred to the more complicated case of a mixture N_2-O_2. The final goal is to understand the behaviour of such plasmas and to obtain the conditions that optimize the plasma sterilization process.

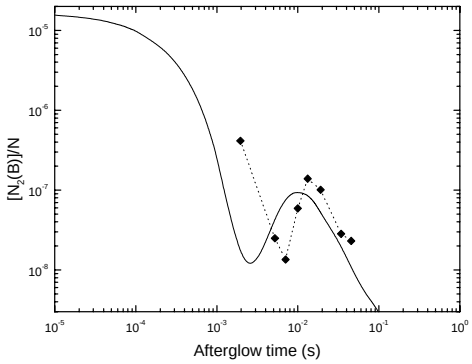

Figure 13.13 – Calculated and measured temporal evolution of the fractional concentration of the $N_2(B)$ radiative state in the afterglow of a microwave nitrogen discharge.

13.3. MODELLING OF PLASMA REACTORS

13.3.1. Introduction

Plasma Reactors (PR) are nowadays an essential tool used in different types of industrial chains with electronics, photovoltaic, optics, food industry, or surface modification. In recent years, new reactor configurations have been proposed in order to give adequate effective answers, according to the objectives of each application.

The main objective with this research line is the development of simulation tools to optimize, in an effective realistic way, the operation conditions of different PR's. The validation of such tools requires a strong interaction between modeling and experiment, without which it will not be possible to improve the understanding of the main mechanisms controlling discharge operation. Such interaction is ensured here through different collaborations with foreign research teams.

13.3.2. Modelling of a capacitively-coupled radio-frequency reactor[5]

Modeling of a capacitively-coupled radio-frequency (ccrf) reactor (Figure 13.14), based on low-pressure (p<1 Torr) pure hydrogen discharges, operating at frequencies up to 80 MHz, has been pursuit.

The systematic characterization of ccrf hydrogen discharges has been achieved, by comparing model results to experimental measurements for various electrical parameters (the self-bias voltage, the plasma potential and impedance, and the power coupled to the plasma), obtained at different rf applied voltages, frequencies and pressures (Figures 13.15 and 13.16). It was possible to simulate and control the development of Double Ionization Structures with hydrogen radio-frequency discharges, by inducing its occurrence in a modified hydrogen-like gas (Figure 13.17).

[4] Also performed in Grenoble, France.

[5] This research was carried out in collaboration with *the Laboratoire de Physique et Technologie des Plasmas*, (LPTP, Palaiseau, France) and the *Laboratoire de Physique des Gaz et des Plasmas* (LPGP, Orsay, France).

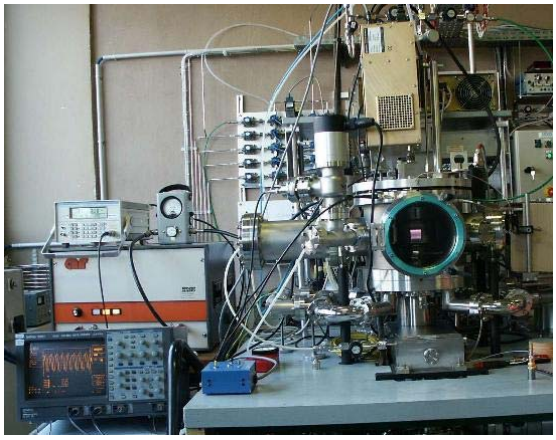

Figure 13.14 – Capacitively coupled radio-frequency reactor, (LPTP, Ecole Polytechnique, Palaiseau, France).

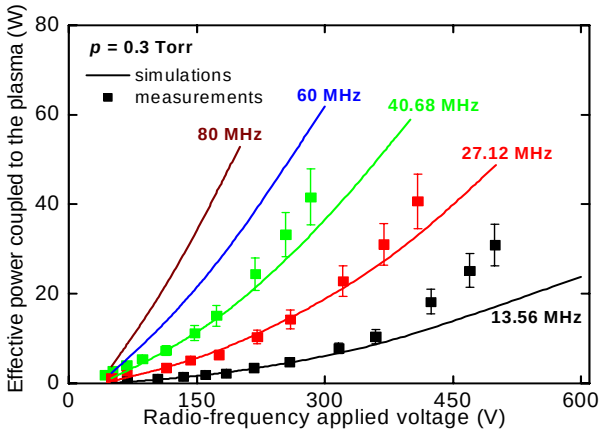

Figure 13.15 – Effective power coupled to the hydrogen plasma.

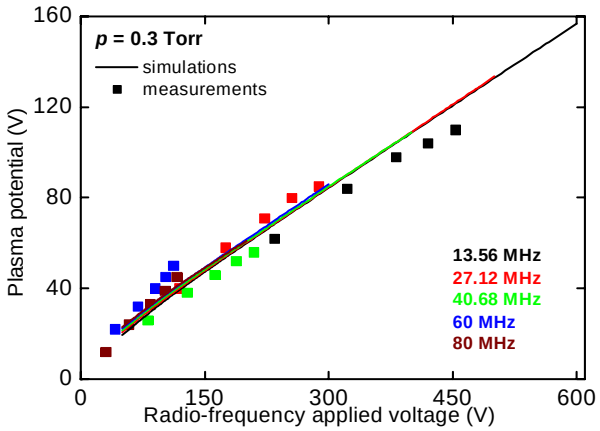

Figure 13.16 – Plasma potential at discharge axis.

The improvement of the comparison between measurements (obtained by probe measurements and LIF) and simulations for the densities of electrons and H-atoms, at different discharge operating conditions has been initiated (Figures 13.18 and 13.19). This goal requires the coupling between (i) a two-dimensional, time-dependent, collisional-radiative model (based on a solution to the Navier-Stokes / Saint-Venant equations), including the reactive multi-component diffusion transport of H(n=1-5) electronically excited atoms and $H_2(X^1\Sigma_g^+,v=0..14)$ vibrationally excited ground state molecules; and (ii) a two-dimensional, time-dependent, fluid code for the transport of charged particles (electrons and H^+, H_2^+, H_3^+ and H ions).

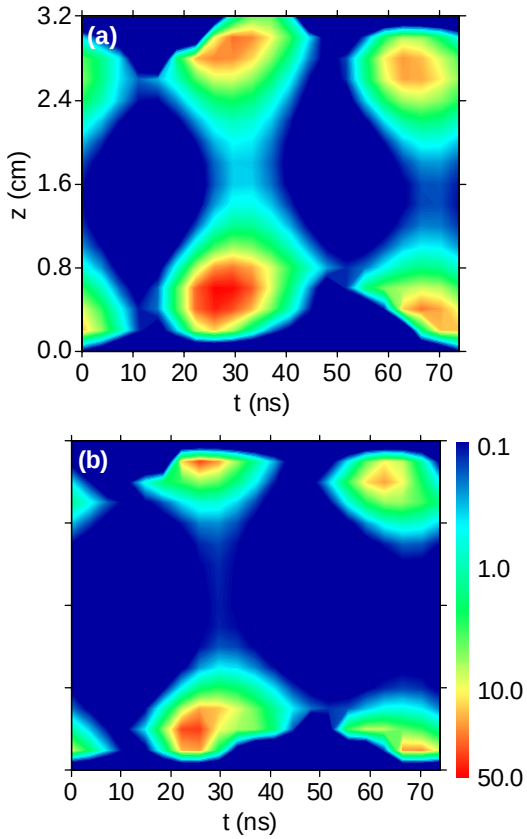

Figure 13.17 – Space-time variation (at discharge axis and during one rf cycle) with the ionization rate (in 10^{14} cm^{-3} s^{-1}), for a ccrf discharge operating at 13.56 MHz frequency, 217 V applied voltage and 1 torr pressure, in (a) standard hydrogen; (b) modified hydrogen adopting $\mu(H_3^+)/10$.

13.3.3. Theoretical and experimental studies of microwave excitation structures

The interplay between modeling and experiment in the characterization of microwave excitation structures, currently used in plasma reactors for thin films deposition, has been intensified. The following activities have been carried out: (i) probe measurements in order to determine, as a function of radial and axial positions, the electron energy distribution function, the electron density and the electron temperature; and (ii) spectroscopy measurements aiming at determining the relative populations of some excited states with the background gas.

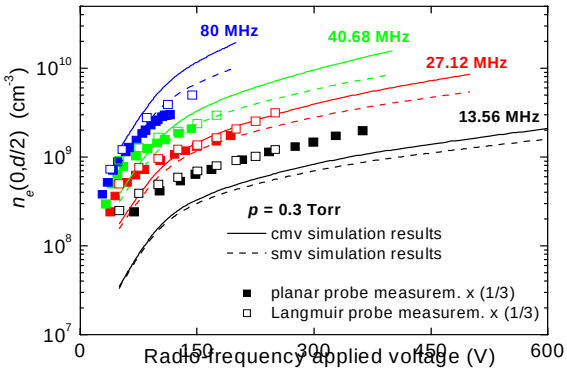

Figure 13.18 – Electron density at discharge axis, obtained with various model versions (cmv and svm).

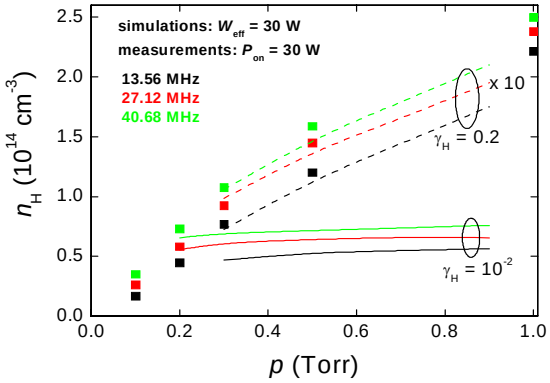

Figure 13.19 – H-atoms density, as a function of pressure, obtained at various wall-recombination coefficients (γ_H).

This task concerned the study of two excitation structures.

(i) A cylindrical excitation structure (corresponding to the sequence plasma-dielectric-air-metal of propagation media, within a 1cm tube radius), operating at 2.45 GHz frequency in argon, for intermediate pressures (~1Torr) and average electron densities around 10^{12} cm^{-3} [6].

(ii) A coaxial excitation structure (corresponding to the sequence metal-air-dielectric-plasma-metal of Torr) and average electron densities bellow 10^{12} cm^{-3} [7].

A collisional-radiative model (CRM) at 30 levels for the argon gas has been developed, proposing a new set of electron collision cross-sections and/or rate coefficients, for the direct and stepwise excitation/de-excitation of argon levels. The CRM results yield a general good agreement with spectroscopic measurements of different line intensity ratios with the 4p and 5p systems (Figure 13.22).

Figure 13.20 – Microwave reactor (cylindrical configuration), (ICMS, Sevilla, Spain).

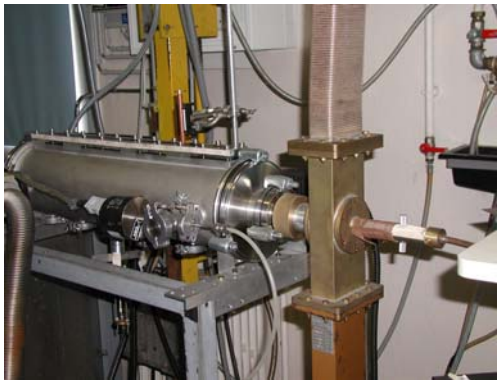

Figure 13.21 – Surface-wave discharge (coaxial configuration), (LPGP, Orsay, France).

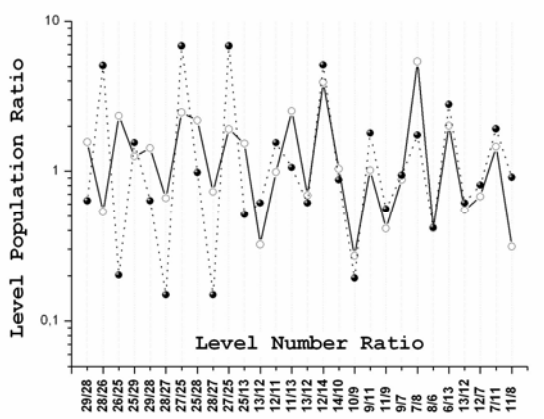

Figure 13.22 – Measured (solid line) and calculated (dashed) line intensity ratios, at 60 mTorr pressure and 400 W power.

[6]This research work was carried out in collaboration with the *Instituto de Ciencias de Materiales de Sevilla* (ICMS, Sevilla, Spain) and the *Facultad de Física* of the *Universidad de Sevilla*, under the framework of the *Acções Integradas Luso-Espanholas* (2003-2004 CRUP – CSIC's agreement, project E-51/02).

[7]This research work was developed in the framework of the *Acções Integradas de Cooperação Científica e Técnica Luso-Francesas* (2004 GRICES – EGIDE's agreement), with the *Laboratoire de Physique des Gaz et des Plasmas* (LPGP, Orsay, France).

Simulation of the electron density and temperature radial distributions within the microwave discharge has been achieved, by using a one-dimensional fluid code for the transport of charged particles. Model results were compared with probe measurements of these quantities (Figures 13.23 and 13.24)

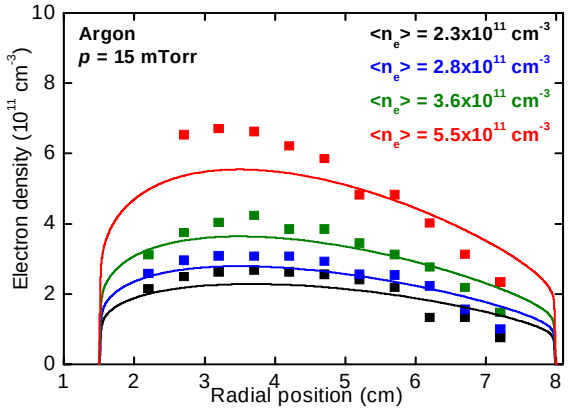

Figure 13.23 – Electron density radial profiles

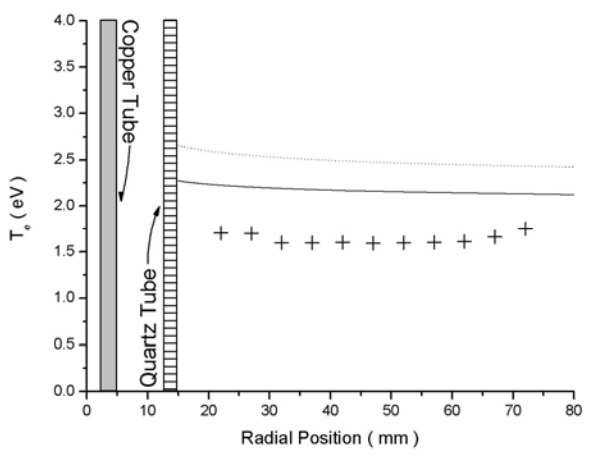

Figure 13.24 – Electron temperature radial profiles, at 30 mTorr pressure and 700 W power. Calculations were obtained with CRM (solid line), and without CRM (dotted).

First experimental evidence has been found, in support of model predictions, of the presence of supra-thermal electrons, issuing from a plasma-resonance region within the space-charge region, near the wall (Figures 13.25 and 13.26).

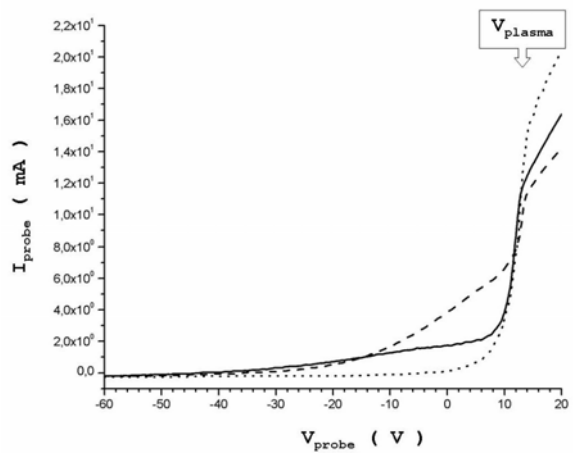

Figure 13.25 – Planar probe characteristics at a constant radial position of 2 mm, for 30 mTorr gas pressure and 200 W power, and for different probe orientations: solid line (radial), dashed (axial) and dotted (azimuthal).

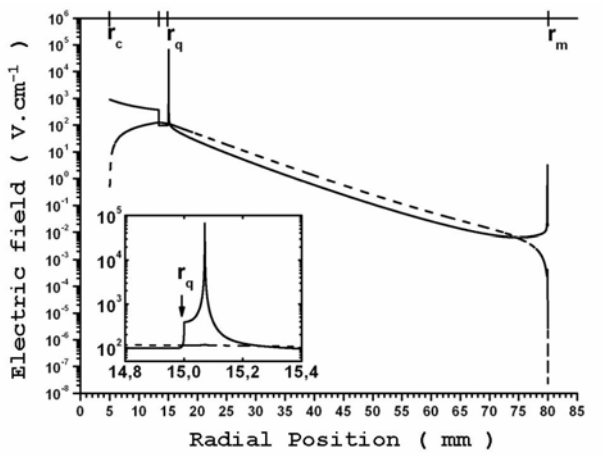

Figure 13.26 – Calculated radial distribution of the wave electric field components (Er, solid line; Ez, dashed), at 30 mTorr pressure and ~ 500 W power. The lower left graph is a blow-up of the inner resonance region.